ACTIVE NOISE CONTROL USING FINITE ELEMENT-BASED VIRTUAL SENSORS

A.P. Berkhoff [1,2] *T. Hekman*[1]

[1] University of Twente, faculty of Engineering Technology, Drienerlolaan 5, 7522 NB Enschede (NL)
[2] TNO Technical Sciences, Acoustics and Sonar, Oude Waalsdorperweg 63, 2597AK Den Haag (NL)

ABSTRACT

This paper describes results of an active noise control system using finite element-based virtual sensors. Systems for active reduction of noise are usually designed to minimize the noise at a physical error sensor. To obtain better noise reduction at a location away from the physical error sensors, virtual sensor techniques have been proposed. These methods require calibration with physical sensors at the monitor sensor location and virtual error sensor location. This can be time-consuming and inconvenient. This paper describes a method in which virtual sensors are determined using a finite element model to eliminate the calibration step. The method is tested in an experimental set-up for a ventilation system with heat recovery. Results are shown, comparing the performance of the finite element based virtual sensor to that of a physical sensor and a measured virtual sensor.

Index Terms— Active noise control, virtual sensors

1. INTRODUCTION

A limitation of active noise control systems is that they obtain their maximum reduction at the locations of the error sensors, with reduction diminishing with increasing distance from the sensors [1]. In practice it is often impractical, or even impossible to place physical microphones at the position where maximum reduction is desired. To overcome this problem, virtual sensor methods have been developed [2]. Several applications for virtual sensors have been researched [3]. The so-called remote microphone technique can be used to implement a virtual sensor [4]. Moving virtual sensors were discussed by Moreau et al. [5]. A Kalman virtual sensor and the remote microphone technique have been compared [6]. A variation of the remote microphone technique is possible, in which the secondary transfer path is split in two parts [7]. Most current virtual sensor methods require a calibration phase, during which the transfer path between the monitor sensor and the virtual sensor location is measured using a physical microphone. This calibration process can be quite intrusive and time consuming. Ideally, the virtual sensor path could be determined without needing to physically measure it. For this study a finite element model of a ventilation duct was created and the virtual sensor path was calculated using a simulation.

The application is related to energy efficient ventilation in buildings. Reduced heat loss in buildings can be obtained by improved insulation, improved airtightness and use of heat recovery [8]. Sufficient ventilation is required in order to guarantee a minimum degree of air quality [9]. To reduce the amount of energy loss through ventilation, these systems can be fitted with heat recovery units [10]. The noise generated by these units and forced ventilation systems in general is often experienced as disturbing, sometimes resulting in users switching the ventilation system to a lower setting, or switching it off completely [11]. However, this obviously reduces the air quality, which is undesired. The sources of ventilation noise are the action of the impeller in air, mechanical vibrations due to the fan and turbulence of the air in the ducts [12]. The noise generated by the latter two sources can be reduced to low levels by proper system design [13]. This is not the case for the acoustic pressure generated by the action of the impeller. The general approach for reducing such disturbances is the application of passive dampers. However, the necessary thickness of damping material depends on the wavelength of the noise [14]. At low frequencies the wavelengths are so long that passive dampers would have to be impractically large to be effective. The dampers can be kept to a practical size by applying active noise control systems to reduce the low-frequency noise.

Noise in ducts is the subject of a large amount of research related to active noise control [15, 16]. Early work is from, e.g., Roure [17], Swinbanks [18], Eriksson [19]. Other experimental work on active reduction of noise from ventilation ducts is described by, e.g., Cochi et al. [20]. A focus of more recent research is the development of a compact configuration, allowing for modular control units [21–23]. Some commercially available modular active noise control units for ventilation systems have been developed [24, 25].

This paper presents a variation of the remote microphone technique [4] in which particular parts of the transfer functions, i.e., the primary and secondary paths of the monitoring sensors to the virtual error [7], are obtained from a finite element model, with the objective to alleviate the requirement to determine the latter transfer paths experimentally. The finite element model could also be used to schedule the virtual sensor paths on flow speed, for example. The transfer paths

thus consist of a part which is obtained experimentally using system identification and a part which is determined from a physical model. This enables compact self-contained control units without wired or wireless sensors at a distance from the unit. The contributions of this paper are the design of an active noise control system for supply vents of ventilation systems with heat recovery and the determination and application of finite element based virtual sensors.

2. METHOD

2.1. Control strategy

A schematic representation of the control system is shown in Fig. 1. The dotted line indicates the separation between the digital and physical domain. Everything inside the line is digital, while everything outside it is physical. G_{dx}, G_{dy} and G_{dz} are defined as the transfer functions between the primary source signal d and its contribution to the reference signal x, the monitor signal e_y and the physical error signal e_z, respectively. G_{ux}, G_{uy} and G_{uz} are the transfer functions between output u of the controller W and its contribution to the reference signal, the monitor signal and the physical error signal, respectively. No feedback is taken into account in the calculation of the controller W. During control, the feedback is compensated using an estimate $\hat{G}_{ux}$ of the feedback path G_{ux}, leading to a version of the reference signal $\hat{x}$ from which the contribution s_x of G_{ux} is removed using the estimate $\hat{s}_x$. Therefore, a good estimate of the feedback path $\hat{G}_{ux}$ is important. H^d_{yz} and H^s_{yz} are the virtual transfer functions between the monitor and error signals for the primary and secondary source, respectively. The virtual sensor paths for the primary and secondary sources are separated, as in the remote microphone technique [4]. In addition, the secondary path from u to the virtual error signal $\hat{e}_z$ is split in two parts G_{uy} and H^d_{yz} [7]. The virtual sensor paths can either be measured or determined using the FEM model. Together with the secondary path estimate $\hat{G}_{uy}$ they are used to calculate the virtual error signal $\hat{e}_z$. The controllers are calculated offline using the reference signal x, a secondary path and a disturbance signal. The last two vary between controllers.

2.2. Finite element model

A finite element model of a part of the duct was created in COMSOL to determine the virtual sensor paths. For this study the model was kept as general as possible and no specific features of the duct layout or the ventilated room were taken into account. In this way the model can be used for different types of ventilation ducts and rooms. The model consists of a single 1 m long straight tube, ending in a 90 degree bend and radiating into an infinite half-space. The model is shown in Fig. 2. The infinite half-space is modeled as a hemisphere, surrounded by a perfectly matched layer (PML) to prevent reflections. The primary source is modeled as an incident plane wave at the other end of the duct. In this way no reflections occur at this end of the duct. The details that are taken into account in the model are the valve covering the outlet opening and the secondary source and its casing. It was found that shortening the straight section in the model does not significantly alter the results. The secondary source is modeled as a normal acceleration on a circular surface equal to the oscillating surface of the actual source. The source and the reference sensors are mounted inside the duct. The monitor sensor is modeled as a point at which the pressure is sampled. The pressure at the error sensor is calculated using far-field calculation [26]. As a result, the size of the hemisphere can remain small. Because the full integral is evaluated, it also enables the user to calculate the pressure at another point in the far field without re-evaluating the model. The location of the secondary source, valve cover and the monitor and error sensors are identical to those in the test set-up. A regularized least-squares method was used to convert the cross- and autospectra of monitoring sensor and error sensor to time domain responses for H^d_{yz} and H^s_{yz}.

3. RESULTS

3.1. Test set-up

A section of cylindrical 125 mm diameter steel ventilation duct was built to demonstrate the effectiveness of the active noise control system, as shown in Fig. 3. The constructed duct consists of three 1 m long tubes, connected by two 90 degree bends. At the outlet, the duct ends with a 90 degree bend and is covered by an adjustable valve (labeled 1 in Fig. 3). A layer of damping material was applied to the valve cover, to prevent it from resonating (not shown in Fig. 3). The dimensions of the duct end is shown in Fig. 5. The default setting of the valve cover was 15 mm away from the wall. This design differs from the layout of an actual ventilation duct in a few significant ways. The most notable difference is the duct length. The short length of the set-up means reflections will occur at the far end of the duct. To attenuate these unwanted reflections, a passive damper was added (labeled 2 in Fig. 3). The spectrum and sound pressure level as used in the experiments are based on the supply of a ventilation system with heat recovery [27] reproduced by a primary source (labeled 3 in Fig. 3). Due to the presence of low frequencies in the ventilation noise, a speaker with adequate low-frequency output is required. A Tang Band W2-2040S 2" sub-woofer was selected. The secondary source (see Fig. 4) is mounted inside the duct. The control algorithm was run on a dSPACE MicroLabBox using a sample rate of 12 kHz. The reference signal was obtained from a combination of two microphones spaced 2.86 cm apart (1 sample) which was used to cancel the upstream acoustic waves. The combined reference signal prevents a performance reduction due to dips in the spectrum of a single reference sensor caused by reflections at the end

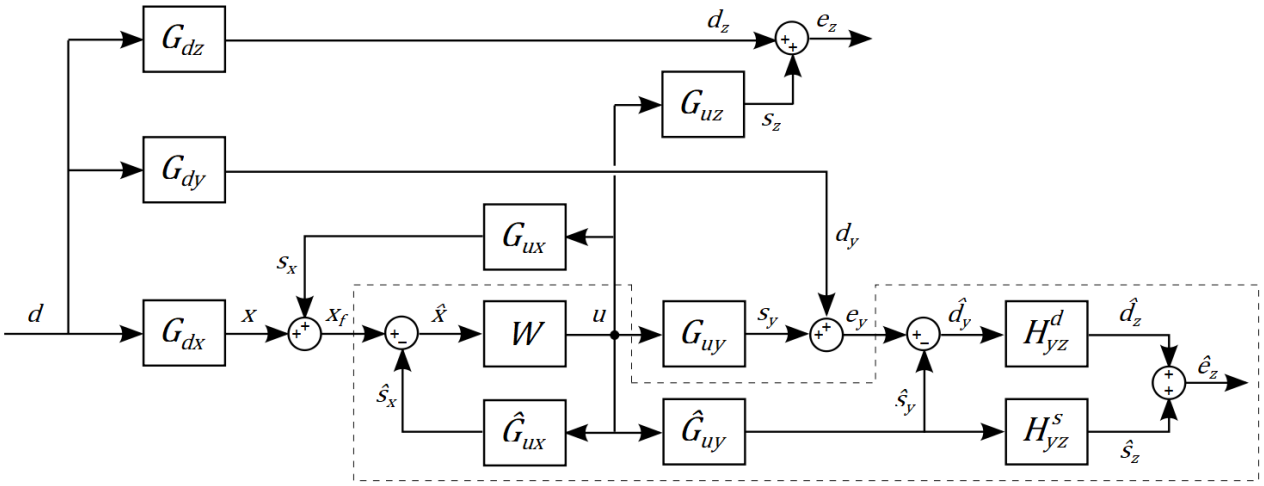

Fig. 1. Schematic representation of the control system. The dotted line denotes the part of the system which exists in the digital domain, while everything outside it exists in the physical domain.

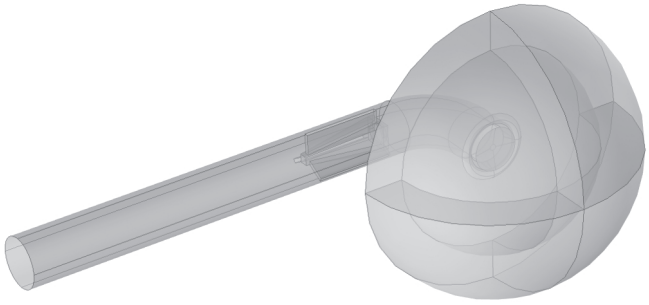

Fig. 2. Finite element model used to determine the virtual sensor paths.

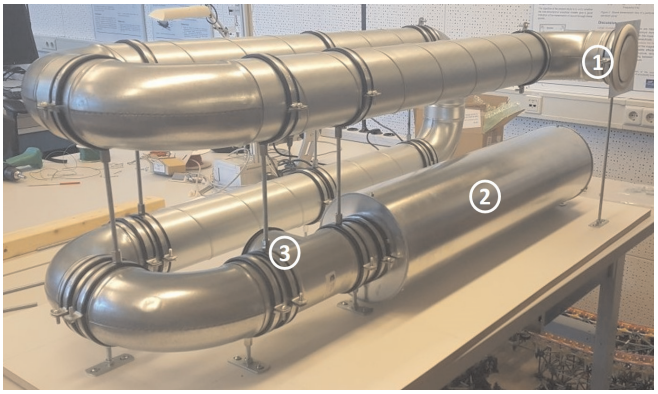

Fig. 3. Ventilation duct built for testing and demonstrating the ANC system. Labeled in the figure are 1) the adjustable valve covering the outlet, 2) the passive damper and 3) the location where the primary source is entered into the duct.

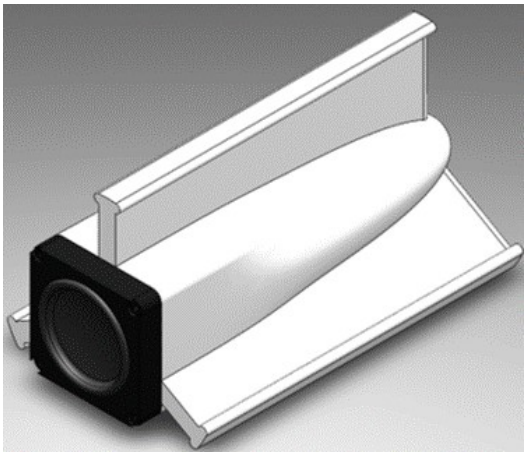

Fig. 4. Secondary source mounted in an aerodynamic casing.

of the duct. The linear time-invariant controller was obtained by minimizing the mean-square value of the error signal for a signal duration of 40 s using a fixed finite impulse response filter with a length of 960 coefficients, leading to a Toeplitz system of equations $Aw = b$, with w the coefficients of W. Increased stability of the controller was obtained with regularization by adding $\beta\bar{A}$ to the diagonal elements of A, with $\bar{A}$ the mean (for multichannel) of the diagonal of A. The regularization coefficient was determined from a tradeoff between performance and condition number of A. The regularization used for the experiments in this paper is $\beta = 10^{-3}$. It was found that the controller emphasized reduction of low frequencies, while reducing less at mid frequencies to which the ear is more sensitive. Therefore, A-weighting was added to the cost functions to take perceived noise into account.

3.2. Noise reduction results

Fig. 6 compares real-time noise reduction results for different error signals to determine the controller. Four error signals

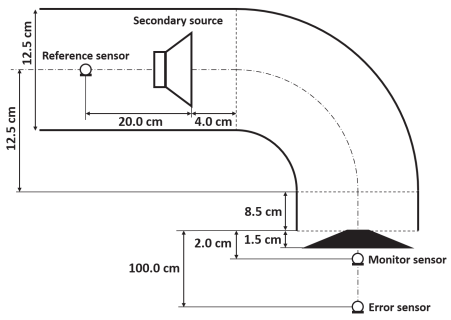

Fig. 5. Diagram of the sensor and source positions in the test set-up.

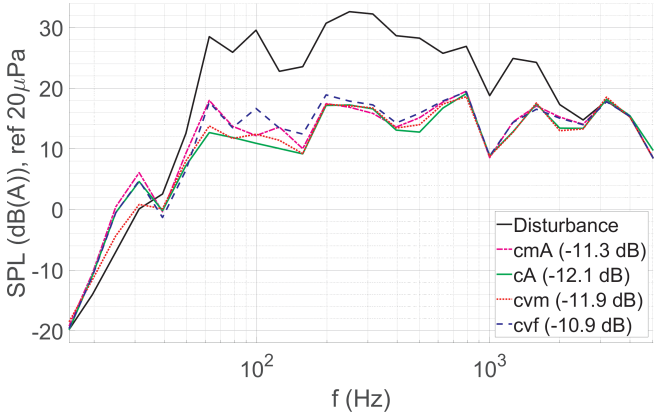

Fig. 6. Average A-weighted sound pressure level per third-octave band at the error sensor when using a combined reference (see text); comparison between results of controllers optimizing the A-weighted monitor signal (cmA), the A-weighted error signal (cA), A-weighted measured virtual sensors (cvm) and A-weighted FEM-based virtual sensors (cvf).

are used: the monitor signal (cmA), the physical error signal (cA), the virtual error signal based on measured transfer functions between monitor signal and error signal (cvm), and the virtual error signal based on finite element-based transfer functions between monitor signal and error signal (cvf). All controllers included A-weighting in the cost function when the control coefficients were determined. Noise reductions were determined from measurements at the physical error sensor position, i.e., the signal e_z. It can be seen that the highest noise reduction of 12.1 dB is obtained by directly minimizing the measured physical error signal. The noise reduction using a measured virtual sensor is only slightly less, being 11.9 dB. The noise reduction of the finite element based virtual sensor is 1 dB less than the measured virtual sensor, being 10.9 dB, which can be explained by the absence of reflections from the test chamber in the finite element model. The noise reduction using the monitor signal as the error signal is 11.3 dB. The results show that the noise reduction obtained with the finite element based virtual sensor is close to the noise reduction obtained with the physical error sensor and the noise reduction obtained with measured virtual sensor, but also to the noise reduction obtained with the monitoring sensor. Because of the single input single output control and the dominant noise being related to one-dimensional sound propagation in the duct, the control results are similar, and therefore the advantage of using a virtual sensor technique can not be clearly demonstrated using the present setup. Some of the control results in Fig. 6 show small increases of the noise at frequencies around 30 Hz. It was found that better performance (not shown in Fig. 6) at these frequencies with similar performance at other frequencies can be obtained by using a second error signal without A-weighting, in addition to the A-weighted error signal. The best performance depends on the relative strength of these two error signals, and was obtained by multiplying the error signal without A-weighting by a factor 1/12. In situations in which the virtual sensor path is subject to large changes the finite element based sensor and the measured virtual sensor could lead to reduced noise reductions. For some situations a scheduling approach could be useful.

4. CONCLUSION

It is shown that for the air supply vent of a ventilation system with heat recovery, using a control device which is mounted inside the duct, the noise reduction obtained with a finite element based virtual sensor is close to the noise reduction obtained with the physical error sensor and the noise reduction obtained with a measured virtual sensor. Although the finite element-based virtual sensor technique led to significant noise reductions, the test setup as used in the paper is not suitable for full validation of the method, and additional experimental work is needed. The finite element-based virtual sensor could have an advantage in applications in which there are multiple monitoring sensors and virtual error sensors, such as when controlling higher order modes radiated from a duct or when noise reduction has to be optimized in a specific direction or region of space, but for which calibration with physical error sensors is undesirable.

5. REFERENCES

[1] S.J. Elliott, P Joseph, A.J. Bullmore, and P.A. Nelson, "Active cancellation at a point in a pure tone diffuse sound field," *J. Sound Vib.*, vol. 120, pp. 183–189, 1988.

[2] P. Albertos and G.C. Goodwin, "Virtual sensors for control applications," *Annual Reviews in Control*, vol. 26, pp. 101–112, 2002.

[3] S.J. Elliott, W. Jung, and J. Cheer, "Head tracking extends local active control of broadband sound to higher frequencies," *Scientific reports*, vol. 8, pp. 5403, 2018.

[4] A. Roure and A. Albarrazin, "The remote microphone technique for active noise control," in *Proceedings of INTER-NOISE and NOISE-CON Congress and Conference*, 1999, p. 12331244.

[5] D. Moreau, B. Cazzolato, and A. Zander, "Active noise control at a moving virtual sensor in three-dimensions," *Acoustics Australia*, vol. 36, pp. 93 – 96, 2008.

[6] P. Booij and A.P. Berkhoff, "Virtual sensors for local, three dimensional, broadband multiple-channel active noise control and the effects on the quiet zones," in *Proceedings ISMA 2010*, 2010, pp. 151–166.

[7] A.P. Berkhoff, "Control strategies for active noise barriers using near-field error sensing," *J. Acoust. Soc. Am.*, vol. 118, pp. 1469–1479, 2005.

[8] D. Bozsaky, "The historical development of thermal insulation materials," *Periodica polytechnica*, vol. 41, pp. 49–56, 2010.

[9] R. Edwards, *Handbook of domestic ventilation*, Butterworth-Heinemann, Oxford, 2002.

[10] A. Litiu, "Ventilation system types in some eu countries," *REHVA Journal*, vol. 01/2012, pp. 18–23, 2012.

[11] W.P. Jongeneel, R.P. Bogers, and I. van Kamp, "Kwaliteit van mechanische ventilatiesystemen in nieuwbouw eengezinswoningen en bewonersklachten, rapport 630789006/2011, https://www.lenteakkoord.nl/wp-content/," 2011.

[12] H.D. Goodfellow and E. Tähti, *Industrial Ventilation Design Guidebook*, Academic Press, London, 2001.

[13] C.M. Harris, *Handbook of noise control*, McGraw-Hill, New York, 1979.

[14] H.V. Fuchs, *Applied acoustics: concepts, absorbers, and silencers for acoustical comfort and noise control*, Springer, Berlin, 2013.

[15] S.M. Kuo and D.R. Morgan, *Active noise control systems*, John Wiley & Sons, New York, 1996.

[16] S.J. Elliott, *Signal Processing for Active Control*, Academic Press, London, 2001.

[17] A. Roure, "Self-adaptive broadband active sound control system," *J. Sound Vib.*, vol. 101, pp. 429–441, 1985.

[18] M.A. Swinbanks, "The active control of sound propagation in long ducts," *J. Sound Vib.*, vol. 27, pp. 411–436, 1973.

[19] L.J. Eriksson and M.C. Allie, "Use of random noise for on-line transducer modeling in an adaptive active attenuation system," *J. Acoust. Soc. Am.*, vol. 85, pp. 797–802, 1989.

[20] A. Cocchi, M Garai, and P. Guidorzi, "Active noise control in heating, ventilation and air conditioning systems," in *Proceedings of 7th International Congress on Sound and Vibration*, 2000.

[21] P. Gardonio and J. Rohlfing, "Modular feed-forward active noise control units for ventilation ducts," *J. Acoust. Soc. Am.*, vol. 136, pp. 3051–3062, 2014.

[22] M. Larsson, S. Johansson, I. Claesson, and L. Håkansson, "A module based active noise control system for ventilation systems, part ii: Performance evaluation," *International Journal of Acoustics and Vibration*, vol. 14, pp. 196–206, 2009.

[23] Fraunhofer-Allianz Adaptronik, "Active noise control modules for ventilation ducts, https://www.adaptronik.fraunhofer.de /en/projects/activnoiseduc .html," 2018.

[24] TechnoFirst, "Ventilation duct noise control: Acta®, retrieved from: http://www.technofirst.com/en/acta-ventilation-duct-noise-control/," 2018.

[25] Silentium, "Active noise reduction, control and cancellation solutions, retrieved from: https://www.silentium.com/," 2018.

[26] COMSOL AB, "Acoustics module user's guide, comsol 5.3a," 2017.

[27] Zehnder Nederland B.V., "Technische specificatie zehnder whr 930, retrieved from: https://www.zehnder.nl/download/6409/74845/20600.pdf," 2018.